Universal image systems for non-periodic and periodic Stokes flows above a no-slip wall

Wen Yan [a,b,*], Michael Shelley [a,b]

[a] *Center for Computational Biology, Flatiron Institute, Simons Foundation, New York 10010, United States of America*
[b] *Courant Institute of Mathematical Sciences, New York University, New York 10012, United States of America*

ARTICLE INFO

ABSTRACT

It is well-known that by placing judiciously chosen image point forces and doublets to the Stokeslet above a flat wall, the no-slip boundary condition can be conveniently imposed on the wall Blake (1971) [8]. However, to further impose periodic boundary conditions on directions parallel to the wall usually involves tedious derivations because single or double periodicity in Stokes flow may require the periodic unit to have no net force, which is not satisfied by the well-known image system. In this work we present a force-neutral image system. This neutrality allows us to represent the Stokes image system in a universal formulation for non-periodic, singly periodic and doubly periodic geometries. This formulation enables the black-box style usage of fast kernel summation methods. We demonstrate the efficiency and accuracy of this new image method with the periodic kernel independent fast multipole method in both non-periodic and periodic geometries. We then extend this new image system to other widely used Stokes fundamental solutions, including the Laplacian of the Stokeslet and the Rotne–Prager–Yamakawa tensor.

© 2018 Elsevier Inc. All rights reserved.

1. Introduction

No-slip boundaries in Stokes flow are central to much flow phenomena. For example, for Brownian suspensions above a no-slip wall, the wall not only constrains the motion of particles, but fundamentally changes the self and collective Brownian motion of suspensions by inducing anisotropy and screening effects in the mobility of particles [1–3]. Another example is that swimming microorganisms may swim upstream near a no-slip boundary in an imposed flow due to either hydrodynamic or non-hydrodynamic causes [4–7].

To compute the Stokes flow above a no-slip wall, the image method of Blake [8] is a popular choice. For a Stokeslet above a wall Blake showed that the no-slip condition was satisfied by adding an image Stokeslet, a modified source doublet, and a modified force doublet to the original Stokeslet. Similar methods have also been developed by Mitchell and Spagnolie [9,10]. Recently, Gimbutas et al. [11] developed a simpler image system. This system invokes standard Stokes and Laplace kernel evaluations only, which is compatible with the Fast Multipole Method (FMM). However, to further impose periodic boundary conditions on the two directions parallel to the no-slip wall is no simple task, because different kernel summations in the image system need to be periodized simultaneously and coupled to each other. Nguyen and Leiderman [12] recently derived the Ewald summation formulation for the doubly periodic Stokeslet image system, but their method showed a non-optimal

---

* Corresponding author at: Center for Computational Biology, Flatiron Institute, Simons Foundation, New York 10010, United States of America.
E-mail addresses: wyan@flatironinstitute.org, wenyan4work@gmail.com (W. Yan), mshelley@flatironinstitute.org (M. Shelley).

$\mathcal{O}(N^2)$ scaling for N point forces. Their method was recently applied in the study of ciliary beating [13]. To our knowledge, the singly periodic Stokeslet image system above a no-slip wall has not yet been derived.

For convenience and efficiency, it is desirable to develop an image system where each kernel sum $\boldsymbol{g}^t = \sum_s \boldsymbol{K}(\boldsymbol{x}^t, \boldsymbol{y}^s)\boldsymbol{q}(\boldsymbol{y}^s)$ can be independently computed and periodized. Here $\boldsymbol{x}^t$ and $\boldsymbol{y}^s$ are target and source points with indices s and t. $\boldsymbol{K}$ is the kernel function. The kernel sum could be simply written as $\boldsymbol{g} = \boldsymbol{K}\boldsymbol{q}$, where the indices s, t are suppressed. For Stokes and Laplace kernel sums, recently developed optimal fast periodic kernel summation methods with flexible periodic boundary conditions can be used, including the Spectral Ewald methods [14–16], which scale as $\mathcal{O}(N \log N)$, and the periodic Kernel Independent Fast Multipole Method (KIFMM) method by Yan and Shelley [17], which scales as $\mathcal{O}(N)$. However the image systems developed by Gimbutas et al. [11] does not work in this framework, because the partially periodic (i.e., simply or doubly periodic) summations for the Stokeslet and the Laplace monopole kernel do not allow a net force or a net monopole in a periodic box, as otherwise the infinite periodic summations diverge. Unfortunately this requirement is not satisfied by the image system of [11].

In this work we propose a new image system for the Stokeslet, which satisfies the neutrality condition by rearranging the Stokeslet and Laplace kernel sums in the image system by Gimbutas et al. [11]. Therefore any singly or doubly periodic kernel summation method can be used as a black-box routine to periodize this new image system.

In Section 2 we briefly derive the new image system. Numerical results for Stokeslet above a no-slip wall with non-periodic and doubly periodic boundary conditions are presented in Section 3. In Section 4 we extend the new image to the Laplacian of Stokeslet and the widely used Rotne–Prager–Yamakawa tensor [18,19]. We conclude this work with a brief discussion about its coupling to fast summation methods, and its extension to other kernels.

2. Formulation

We first consider a point force $\boldsymbol{f} = (f_1, f_2, f_3)$ located at $\boldsymbol{y} = (y_1, y_2, y_3)$ above an infinite no-slip wall at the plane $x_3 = 0$. We define the image force $\boldsymbol{f}^I = (f_1, f_2, -f_3)$ located at $\boldsymbol{y}^I = (y_1, y_2, -y_3)$ below the wall. The complete image system to satisfy the no-slip condition on the wall is given by Gimbutas et al. [11] following the Papkovich–Neuber technique:

$$\boldsymbol{u}(\boldsymbol{x}) = \boldsymbol{J}(\boldsymbol{x}, \boldsymbol{y})\boldsymbol{f} + \boldsymbol{J}(\boldsymbol{x}, \boldsymbol{y}^I)\left(-\boldsymbol{f}^I\right) - \boldsymbol{u}^C(\boldsymbol{x}), \tag{1a}$$

$$\boldsymbol{u}^C(\boldsymbol{x}) = x_3 \nabla_x \phi(\boldsymbol{x}) - \hat{\boldsymbol{x}}_3 \phi(\boldsymbol{x}), \quad \phi(\boldsymbol{x}) \stackrel{\text{def}}{=} G^S(\boldsymbol{x}, \boldsymbol{y}^I)f_3^I + \boldsymbol{G}^D(\boldsymbol{x}, \boldsymbol{y}^I)(y_3 \boldsymbol{f}^I), \tag{1b}$$

where $\hat{\boldsymbol{x}}_3$ is the unit vector in the x_3 direction. In this expression three kernels are involved: the Laplace monopole kernel $G^S(\boldsymbol{x}, \boldsymbol{y}) = \frac{1}{4\pi}\frac{1}{|\boldsymbol{x}-\boldsymbol{y}|}$, the Laplace dipole kernel $\boldsymbol{G}^D(\boldsymbol{x}, \boldsymbol{y}) = \frac{1}{4\pi}\frac{\boldsymbol{x}-\boldsymbol{y}}{|\boldsymbol{x}-\boldsymbol{y}|^3} = \nabla_y G^S(\boldsymbol{x}, \boldsymbol{y})$, and the Stokeslet $\boldsymbol{J}(\boldsymbol{x}, \boldsymbol{y}) = \frac{1}{8\pi}\left(\frac{\boldsymbol{I}}{|\boldsymbol{x}-\boldsymbol{y}|} + \frac{(\boldsymbol{x}-\boldsymbol{y})(\boldsymbol{x}-\boldsymbol{y})}{|\boldsymbol{x}-\boldsymbol{y}|^3}\right)$. We set the fluid viscosity to $\eta = 1$ in $\boldsymbol{J}$ for simplicity. It is clear that the net force is $\boldsymbol{f} + (-\boldsymbol{f}^I) = (0, 0, 2f_3) \neq 0$ in the Stokes kernel sum, and the net monopole is $f_3^I = -f_3 \neq 0$ in the Laplace monopole kernel sum. This forbids us to apply partially periodic kernel sum methods directly. The requirement of neutrality is straightforward to understand for Laplace kernels. For Stokeslet this depends on the particular periodic boundary condition. With triply periodic periodic boundary condition, the net force within a periodic box does not have to be zero because the net force can be balanced by the global pressure gradient [20]. However the net force must be zero with singly and doubly periodic boundary conditions, as demonstrated by Lindbo and Tornberg [14].

To remove the net force and net monopole, we convert the third component of Stokes force into a Laplace monopole kernel sum following the idea of Tornberg and Greengard [21]. This involves tedious algebraic manipulations and we only summarize the results here. The new image system splits the flow velocity into 4 independent parts $\boldsymbol{u}(\boldsymbol{x}) = \boldsymbol{u}^S + \boldsymbol{u}^D + \boldsymbol{u}^{L1} + \boldsymbol{u}^{L2}$, where each part is computed by one kernel sum. In the following, $\boldsymbol{f}_{xy} = (f_1, f_2, 0)$ denotes the x_1, x_2 components of the point force $\boldsymbol{f}$, parallel to the no-slip wall.

$$\boldsymbol{u}^S = \boldsymbol{J}(\boldsymbol{x}, \boldsymbol{y})\boldsymbol{f}_{xy} + \boldsymbol{J}(\boldsymbol{x}, \boldsymbol{y}^I)\left(-\boldsymbol{f}_{xy}\right), \tag{2a}$$

$$\boldsymbol{u}^D = \left(x_3 \nabla_x - \hat{\boldsymbol{x}}_3\right)\phi^D(\boldsymbol{x}), \quad \text{with } \phi^D \stackrel{\text{def}}{=} \boldsymbol{G}^D(\boldsymbol{x}, \boldsymbol{y}^I) \cdot y_3(-f_1, -f_2, f_3)^T \tag{2b}$$

$$\boldsymbol{u}^{L1} = -\frac{1}{2}\left(x_3 \nabla_x - \hat{\boldsymbol{x}}_3\right)\phi^S(\boldsymbol{x}), \quad \text{with } \phi^S(\boldsymbol{x}) \stackrel{\text{def}}{=} G^S(\boldsymbol{x}, \boldsymbol{y})f_3 + G^S(\boldsymbol{x}, \boldsymbol{y}^I)(-f_3), \tag{2c}$$

$$\boldsymbol{u}^{L2} = \frac{1}{2}\nabla_x \phi^{SZ}(\boldsymbol{x}), \quad \text{with } \phi^{SZ}(\boldsymbol{x}) \stackrel{\text{def}}{=} \left[G^S(\boldsymbol{x}, \boldsymbol{y})(f_3 y_3) + G^S(\boldsymbol{x}, \boldsymbol{y}^I)(-f_3 y_3)\right]. \tag{2d}$$

$\boldsymbol{u}^S$ denotes the Stokes kernel sum, ϕ^D denotes the Laplace dipole sum, and ϕ^S, ϕ^{SZ} denote two Laplace monopole sums. The values and gradients of ϕ^D, ϕ^S and ϕ^{SZ} are computed at the target point $\boldsymbol{x}$. It is straightforward to verify that $\boldsymbol{u}(\boldsymbol{x})$ is equivalent to the original image system in Eq. (1). In this new image system, the Stokeslet sum and the two Laplace monopole sums are obviously neutral. The Laplace dipole sum is intrinsically neutral, because each dipole source is the asymptotic limit of zero distance between equal and opposite charges. Therefore, each of the 4 kernel sums can be separately periodized, and we claim this new image system is applicable for non-periodic, singly periodic and doubly periodic systems.

Table 1

Timing (in seconds) results for 97^3 target and source points with doubly periodic boundary condition. τ_{tree} is the time to construct the octree for FMM, $\tau_{\mathcal{N}}$ is the time for near-field evaluations and $\tau_{\mathcal{F}}$ is the time for far-field evaluations. Stokes, Dipole, Monopole 1 and Monopole 2 correspond to $\boldsymbol{u}^S$, $\boldsymbol{u}^D$, $\boldsymbol{u}^{L1}$, and $\boldsymbol{u}^{L2}$ in Eq. (2), respectively. p is the number of equivalent points per cubic box edge in KIFMM, controlling the accuracy and cost of KIFMM.

p	Stokes			Dipole & Monopole 1			Monopole 2		
	τ_{tree}	$\tau_{\mathcal{N}}$	$\tau_{\mathcal{F}}$	τ_{tree}	$\tau_{\mathcal{N}}$	$\tau_{\mathcal{F}}$	τ_{tree}	$\tau_{\mathcal{N}}$	$\tau_{\mathcal{F}}$
6	0.75	1.56	0.026	0.81	1.08	0.021	0.81	1.02	0.022
8	0.70	2.03	0.051	0.75	1.43	0.041	0.69	1.37	0.042
10	0.73	2.64	0.085	0.69	1.78	0.068	0.62	1.55	0.066
12	0.73	3.83	0.14	0.67	2.20	0.099	0.90	2.01	0.098
14	0.74	5.14	0.19	0.63	2.59	0.14	0.91	2.38	0.15
16	0.86	7.95	0.28	0.78	3.19	0.18	0.95	2.82	0.18

Eq. (2) obviously keeps the same computational complexity of the underlying summation methods, which is $\mathcal{O}(N \log N)$ for FFT-based methods and $\mathcal{O}(N)$ for KIFMM. Eq. (2) is also close-to-optimal because although one more G^S kernel sum is invoked compared to the image system given by Eq. (1), this G^S kernel sum is usually much faster than the sum for the Stokeslet $\boldsymbol{J}$, because the kernel G^S is a scalar while the Stokeslet $\boldsymbol{J}$ is a 3×3 tensor.

3. Numerical results

In this section we present numerical results using the periodic KIFMM method developed in our previous work [17]. It works by splitting the infinite periodic domain into a near field and a far field. The near field is directly summed by KIFMM while the far field is added through a precomputed Multipole-To-Local (M2L) operator applied to the near field calculation results. A single parameter p controls the accuracy and cost the KIFMM method, by placing p equivalent points per edge, in total $6(p-1)^2 + 2$ equivalent point sources for each cubic box in the octree in the KIFMM algorithm. Using larger p gives better accuracy but has higher computational cost. Approximately, $p = 10$ gives single precision accuracy and $p = 16$ gives double precision accuracy. The M2L operators for the kernels $\boldsymbol{J}$, G^S, and $\boldsymbol{G}^D$ are constructed with the doubly periodic formulation derived by Lindbo and Tornberg [14] and Tornberg [22]. The computer program is based on the high-performance package PVFMM developed by Malhotra and Biros [23]. Since the gradient of Laplace dipole potential and Laplace monopole potential are required in Eq. (2b), (2c), (2d), we modified the corresponding kernels to generate the potentials simultaneously with the gradients in the final Source-To-Target (S2T), Local-To-Target (L2T), and Multipole-To-Target (M2T) stages of KIFMM [24].

We further optimized the implementation by combining Eq. (2b), (2c) into one KIFMM because they share the same operator $(x_3 \nabla_x - \hat{\boldsymbol{x}}_3)$ in the final assembling step. This optimization is achieved by representing the M2M, M2L, and L2L operations in the tree with Laplace monopole densities only.

3.1. Timing results

The computation is timed on a 12-core 3.6 GHz Intel Xeon workstation. 97^3 point forces are placed at a set of random source points. Each force component is randomly generated from a uniform distribution in $[-0.5, 0.5]$, and each coordinate component of the source points is randomly generated from a lognormal distribution with standard parameters $(0.2, 0.5)$. The target points are chosen to be a set of 97^3 Chebyshev quadrature points. The source and target points are both scaled and shifted to fill the half unit cube $[0, 1)^2 \times [0, 0.5)$. The no-slip boundary condition is imposed on the plane $x_3 = 0$ by placing the image points in the other half unit cube $[0, 1)^2 \times (-0.5, 0]$.

With the image method, to evaluate the velocity at T points due to S point forces, the Stokes FMM evaluates from $2S$ source points (including image points) to T target points. The Laplace dipole FMM is from S to T points, and the two Laplace FMMs are both from $2S$ (including image points) to T points. The timing results are shown in Table 1. The Stokes FMM evaluates Eq. (2a) and the Monopole 2 FMM evaluates Eq. (2d). The Dipole & Monopole 1 FMM evaluates both Eq. (2b), (2c) in a single operation, as explained in the optimization mentioned above.

3.2. Accuracy results

In this section we use the same set of point forces and target points in the unit cube as in the last section, and present results for both non-periodic and doubly periodic boundary conditions. To measure the accuracy of satisfying the no-slip boundary condition, a mesh of 97^2 Chebyshev points is placed on the no-slip wall and the maximum component of flow velocity $\max|\boldsymbol{u}|$ at these points is calculated. To measure the accuracy of the doubly periodic boundary condition, a mesh of 97^2 Chebyshev points is placed on each of the four side boundaries with $x_3 \in [0, 0.5]$. The relative L_2 error for the flow velocity at the Chebyshev points on the two side walls $x_1 = 0, 1, x_2 \in [0, 1), x_3 \in [0, 0.5]$ is used as the measurement of periodic boundary condition error in the X direction, denoted by $\epsilon_{L2,X}$. Similarly $\epsilon_{L2,Y}$ is also measured. As shown in Fig. 1 the numerical errors in the no-slip and periodic boundary conditions converge exponentially with increasing p, and close to machine precision can be achieved.
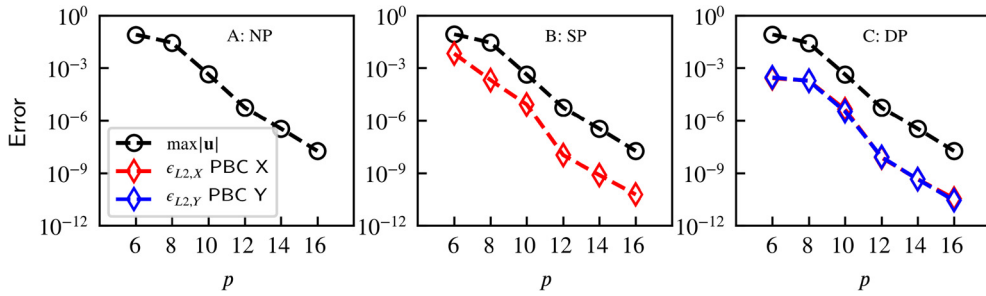
Fig. 1. The accuracy test for the same set of source and target points specified in Section 3.1. A: only no-slip condition is imposed on the $x_3 = 0$ plane. B: singly periodic boundary condition is imposed in x_1 direction. C: doubly periodic boundary condition is imposed in x_1, x_2 directions. In subplot C, $\epsilon_{L2,X}$ and $\epsilon_{L2,Y}$ almost overlap. (For interpretation of the colors in the figure(s), the reader is referred to the web version of this article.)

4. The extension to other Stokes-related kernels

4.1. The Laplacian of Stokeslet

The Laplacian of the Stokeslet, $\nabla_x^2 \boldsymbol{J}$, is often invoked to compute the flow induced by a degenerate force doublet. For example, the flow induced by a slender fiber with length L can be written as $\boldsymbol{u}(\boldsymbol{x}) = \int_{s=0}^{L} \left(1 + \frac{1}{2}\epsilon^2 \nabla_x^2\right) \boldsymbol{J}\left[\boldsymbol{x}, \boldsymbol{y}(s)\right] \boldsymbol{f}(s)$, where $\boldsymbol{f}$ is the force density on the fiber, and $\epsilon \ll 1$ is the slenderness parameter of the fiber [25,26]. It is straightforward to construct the image system for $\nabla_x^2 \boldsymbol{J}$ by directly taking the Laplacian of Eq. (2). However, a simpler image system can be derived by realizing that $\nabla_x^2 \boldsymbol{J}(\boldsymbol{x}, \boldsymbol{y}) = \nabla_x \boldsymbol{G}^D(\boldsymbol{x}, \boldsymbol{y})$. We denote this kernel by $\boldsymbol{Q}(\boldsymbol{x}, \boldsymbol{y})$ because it is similar to the Green's function of an electrostatic quadrupole:

$$\boldsymbol{Q}(\boldsymbol{x}, \boldsymbol{y}) = \nabla_x^2 \boldsymbol{J}(\boldsymbol{x}, \boldsymbol{y}) = \nabla_x \boldsymbol{G}^D(\boldsymbol{x}, \boldsymbol{y}) \tag{3}$$

It is straightforward to verify that $\nabla_x^2 \boldsymbol{Q} = 0$ and $\nabla_x \cdot \boldsymbol{Q} = 0$.

Following the Papkovich–Neuber approach as used by Gimbutas et al. [11], we find a harmonic potential $\phi^{GD} \overset{\text{def}}{=} \hat{\boldsymbol{x}}_3 \cdot [\boldsymbol{Q}(\boldsymbol{x}, \boldsymbol{y}^I) \boldsymbol{f}^I]$ to construct the solution to Stokes equation to complete the image system. We choose the superscript GD because $\boldsymbol{Q}$ is the gradient of the Laplace dipole kernel $\boldsymbol{G}^D$. It is straightforward to verify that the following image system satisfies the no-slip boundary condition and the Stokes equation:

$$\boldsymbol{u}^{GD}(\boldsymbol{x}) = x_3 \nabla_x \phi^{GD}(\boldsymbol{x}) - \hat{\boldsymbol{x}}_3 \cdot \phi^{GD}(\boldsymbol{x}), \quad \phi^{GD}(\boldsymbol{x}) \overset{\text{def}}{=} \hat{\boldsymbol{x}}_3 \left[\boldsymbol{Q}(\boldsymbol{x}, \boldsymbol{y}^I) \boldsymbol{f}^I\right] \tag{4}$$

$$\boldsymbol{u} = \boldsymbol{Q}(\boldsymbol{x}, \boldsymbol{y}) \boldsymbol{f} - \boldsymbol{Q}(\boldsymbol{x}, \boldsymbol{y}^I) \boldsymbol{f}^I - 2\boldsymbol{u}^{GD}, \quad p = -4\frac{\partial \phi^{GD}(\boldsymbol{x})}{\partial x_3} \tag{5}$$

This image system can be calculated with two kernel sums, $\boldsymbol{Q}(\boldsymbol{x}, \boldsymbol{y})\boldsymbol{f}$ and $\boldsymbol{Q}(\boldsymbol{x}, \boldsymbol{y}^I)\boldsymbol{f}^I$, both involving the $\boldsymbol{Q}$ kernel only. Further we do not need to rearrange and neutralize the sums, because $\boldsymbol{Q}(\boldsymbol{x}, \boldsymbol{y}) = \nabla_x \boldsymbol{G}^D(\boldsymbol{x}, \boldsymbol{y})$ and $\boldsymbol{G}^D$ is intrinsically neutral since it represents a Laplace dipole as discussed before. The doubly periodic formulation by Bleibel [27] or the general formulation for electrostatic systems by Tornberg [22] can be directly used as black-box periodic summation routines for the kernel $\boldsymbol{Q}$.

4.2. The Rotne–Prager–Yamakawa tensor

The Rotne–Prager–Yamakawa (RPY) tensor [18,19] is widely used in simulations of Brownian suspensions and Langevin dynamics of biomolecules because it is a reasonably accurate approximation to hydrodynamics in Stokes flow and, more importantly, is designed to be always symmetric positive definite. Without the wall, the RPY tensor is constructed from the Stokeslet $\boldsymbol{J}(\boldsymbol{x}, \boldsymbol{y})$ as:

$$\boldsymbol{u} = \left(1 + \frac{1}{6}a^2 \nabla_x^2\right) \boldsymbol{u}', \quad \boldsymbol{u}' = \left(1 + \frac{1}{6}b^2 \nabla_y^2\right) \boldsymbol{J}(\boldsymbol{x}, \boldsymbol{y}) \boldsymbol{f}. \tag{6}$$

Here $\boldsymbol{u}'$ is the velocity disturbance induced by the force $\boldsymbol{f}$ on a 'source' particle with radius b, and $\boldsymbol{u}$ is the velocity of a 'target' particle with radius a induced by $\boldsymbol{u}'$. The Laplacian terms $\frac{1}{6}a^2 \nabla_x^2$ and $\frac{1}{6}b^2 \nabla_y^2$ represent the finite-size effects of the target and source particles, respectively. In the absence of the wall, the bi-Laplacian term $\nabla_x^2 \nabla_y^2 \boldsymbol{J}(\boldsymbol{x}, \boldsymbol{y})$ is zero. However, the bi-Laplacian term is not zero in the presence of the wall, and the image system is significantly more complicated than Eq. (6), as shown by Swan and Brady [28]. In this section we derive an image system for Eq. (6) based on Eq. (2). This new image system is applicable with either periodic or non-periodic geometries.

Table 2
The kernel sums for the image RPY tensor in a monodisperse system.

	Source strength and location	Target values
Stokes 1 u^S	f_{xy} at y, and $-f_{xy}$ at y^I	$u^S, \nabla_x^2 u^S$
Laplace Monopole 1 ϕ^S	f_3 at y, and $-f_3$ at y^I	$\phi^S, \nabla_x \phi^S, \nabla_x \nabla_x \phi^S$
Laplace Monopole 2 ϕ^{SZ}	$f_3 y_3$ at y, and $-f_3 y_3$ at y^I	$\phi^{SZ}, \nabla_x \phi^{SZ}, \nabla_x \nabla_x \phi^{SZ}$
Laplace Dipole 1 ϕ^D	$y_3(-f_1, -f_2, f_3)^T$ at y^I	$\phi^D, \nabla_x \phi^D, \nabla_x \nabla_x \phi^D$
Laplace Dipole 2 ϕ^{DZ}	$(0, 0, f_3)^T$ at y, and $(0, 0, f_3)^T$ at y^I	$\nabla_x \phi^{DZ}$
Laplace Quadrupole ϕ^Q	$2\begin{bmatrix} f_3 & 0 & 0 \\ 0 & f_3 & 0 \\ f_1 & f_2 & 0 \end{bmatrix}$ at y	$\phi^Q, \nabla_x \phi^Q$

Starting from Eq. (2), the velocity u of the target particle at x induced by the force f on the source particle located at y is:

$$u = \left(1 + \frac{1}{6}a^2\nabla_x^2\right)u', \quad u' = \left(1 + \frac{1}{6}b^2\nabla_y^2\right)\left(u^S + u^D + u^{L1} + u^{L2}\right). \tag{7}$$

This can be simplified by realizing that $\nabla_y^2 u^{L1} = 0$, $\nabla_x^2 u^{L2} = 0$, and $\nabla_x^2 \nabla_y^2 u^S = 0$:

$$u = u^S + u^D + u^{L1} + u^{L2} + \frac{b^2}{6}\nabla_y^2\left(u^S + u^D + u^{L2}\right)$$

$$+ \frac{a^2}{6}\nabla_x^2\left(u^S + u^D + u^{L1}\right) + \frac{a^2 b^2}{36}\nabla_x^2\nabla_y^2 u^D. \tag{8}$$

The ∇_x^2 terms can be written as:

$$\nabla_x^2 u^S = Q(x, y)f_{xy} + Q(x, y^I)(-f_{xy}), \tag{9}$$

$$\nabla_x^2 u^D = x_3\nabla_x\nabla_x^2\phi^D + 2\frac{\partial}{\partial x_3}\nabla_x\phi^D - [0, 0, \nabla_x^2\phi^D] = 2\frac{\partial}{\partial x_3}\nabla_x\phi^D, \tag{10}$$

$$\nabla_x^2 u^{L1} = -\frac{1}{2}x_3\nabla_x\nabla_x^2\phi^S - \frac{\partial}{\partial x_3}\nabla_x\phi^S - [0, 0, \nabla_x^2\phi^S] = -\frac{\partial}{\partial x_3}\nabla_x\phi^S, \tag{11}$$

where we have utilized the fact that $\nabla_x^2\phi^D = 0$, and $\nabla_x^2\phi^S = 0$.

By symmetry $\nabla_y^2 u^S = \nabla_x^2 u^S$. Other ∇_y^2 and the bi-Laplacian terms can be written as:

$$\nabla_y^2 u^{L2} = \nabla_x\phi^{DZ}, \quad \phi^{DZ} \overset{\text{def}}{=} G^D(x, y) \cdot (0, 0, f_3)^T + G^D(x, y^I) \cdot (0, 0, f_3)^T, \tag{12}$$

$$\nabla_y^2 u^D = x_3\nabla_x\nabla_y^2\phi^D - (0, 0, \nabla_y^2\phi^D), \tag{13}$$

$$\nabla_x^2\nabla_y^2 u^D = 2\frac{\partial}{\partial x_3}\nabla_x\nabla_y^2\phi^D, \quad \nabla_y^2\phi^D \overset{\text{def}}{=} \phi^Q = G^Q(x, y) : 2\begin{bmatrix} f_3 & 0 & 0 \\ 0 & f_3 & 0 \\ f_1 & f_2 & 0 \end{bmatrix}, \tag{14}$$

where $\nabla_y^2\phi^D$ is represented by the field ϕ^Q induced by a Laplace quadrupole with kernel function $G^Q(x, y) = \nabla_y G^D(x, y)$. Here the symbol ': ' denotes double-contraction of 3×3 tensors. The image system for the RPY tensor in non-periodic and periodic geometries can be universally represented as a combination of the terms derived above. We summarize the results for monodisperse and polydisperse systems separately in the following, because in monodisperse systems the image system can be simplified with $a = b$.

*4.2.1. The kernel sums for monodisperse systems*

Using that in monodisperse systems $b = a$ for all particles, the particle radius a is scaled out of the source strengths and 6 kernel sums are needed as shown in Table 2.

The velocity of the target particle can be written as a combination of the target values:

$$u = \left(1 + \frac{a^2}{3}\nabla_x^2\right)u^S + \left(x_3\nabla_x - \hat{x}_3 + \frac{a^2}{3}\frac{\partial}{\partial x_3}\nabla_x\right)\phi^D - \frac{1}{2}\left(x_3\nabla_x - \hat{x}_3 + \frac{a^2}{3}\frac{\partial}{\partial x_3}\nabla_x\right)\phi^S$$

$$+ \frac{1}{2}\nabla_x\phi^{SZ} + \frac{a^2}{6}\nabla_x\phi^{DZ} + \left(\frac{a^2}{6}x_3\nabla_x - \frac{a^2}{6}\hat{x}_3 + \frac{a^4}{18}\frac{\partial}{\partial x_3}\nabla_x\right)\phi^Q \tag{15}$$

Table 3
The kernel sums for the image RPY tensor in a polydisperse system.

	Source strength and location	Target values
Stokes 1 $\boldsymbol{u}^S$	$\boldsymbol{f}_{xy}$ at $\boldsymbol{y}$, and $-\boldsymbol{f}_{xy}$ at $\boldsymbol{y}^I$	$\boldsymbol{u}^S, \nabla_x^2 \boldsymbol{u}^S$
Stokes 2 $\boldsymbol{u}_b^S$	$b^2 \boldsymbol{f}_{xy}$ at $\boldsymbol{y}$, and $-b^2 \boldsymbol{f}_{xy}$ at $\boldsymbol{y}^I$	$\nabla_x^2 \boldsymbol{u}_b^S$
Laplace Monopole 1 ϕ^S	f_3 at $\boldsymbol{y}$, and $-f_3$ at $\boldsymbol{y}^I$	$\phi^S, \nabla_x \phi^S, \nabla_x \nabla_x \phi^S$
Laplace Monopole 2 ϕ^{SZ}	$f_3 y_3$ at $\boldsymbol{y}$, and $-f_3 y_3$ at $\boldsymbol{y}^I$	$\phi^{SZ}, \nabla_x \phi^{SZ}, \nabla_x \nabla_x \phi^{SZ}$
Laplace Dipole 1 ϕ^D	$y_3(-f_1, -f_2, f_3)^T$ at $\boldsymbol{y}^I$	$\phi^D, \nabla_x \phi^D, \nabla_x \nabla_x \phi^D$
Laplace Dipole 2 ϕ_b^{DZ}	$b^2(0,0,f_3)^T$ at $\boldsymbol{y}$, and $b^2(0,0,f_3)^T$ at $\boldsymbol{y}^I$	$\nabla_x \phi_b^{DZ}$
Laplace Quadrupole ϕ_b^Q	$2\,b^2 \begin{bmatrix} f_3 & 0 & 0 \\ 0 & f_3 & 0 \\ f_1 & f_2 & 0 \end{bmatrix}$ at $\boldsymbol{y}$	$\phi_b^Q, \nabla_x \phi_b^Q$
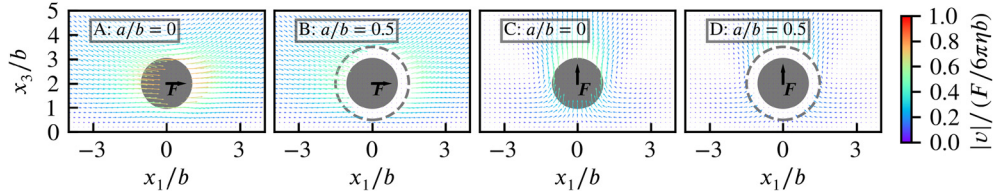
Fig. 2. The velocity of a target particle induced by a source particle. The particle shown in the figure is the source particle with radius b, and a force F is applied on the source particle in $\hat{\boldsymbol{x}}_1$ (A, B) or $\hat{\boldsymbol{x}}_3$ (C, D) directions. The vector field shows the velocity of the target particle with radius a centered at some point in space. A and C: $a/b = 0$, the target particle is infinitely small. B and D: $a/b = 0.5$, the target particle center is not allowed to enter the dashed circle with radius $a + b$ due to non-overlap condition.

4.2.2. The kernel sums for polydisperse systems

In this case we cannot simply scale the kernel sum results with the particle radius as in the previous case because the radius b can be different for all source particles. Therefore b must be included in the source strengths and 7 kernel sums are needed, as shown in Table 3.

The velocity of the target particle is a combination of the target values:

$$\boldsymbol{u} = \left(1 + \frac{a^2}{6}\nabla_x^2\right)\boldsymbol{u}^S + \frac{1}{6}\nabla_x^2 \boldsymbol{u}_b^S + \left(x_3 \nabla_x - \hat{\boldsymbol{x}}_3 + 2\frac{a^2}{6}\frac{\partial}{\partial x_3}\nabla_x\right)\phi^D - \frac{1}{2}\left(x_3 \nabla_x - \hat{\boldsymbol{x}}_3 + 2\frac{a^2}{6}\frac{\partial}{\partial x_3}\nabla_x\right)\phi^S$$
$$+ \frac{1}{2}\nabla_x \phi^{SZ} + \frac{1}{6}\nabla_x \phi_b^{DZ} + \left(\frac{1}{6}x_3 \nabla_x - \frac{1}{6}\hat{\boldsymbol{x}}_3 + \frac{a^2}{18}\frac{\partial}{\partial x_3}\nabla_x\right)\phi_b^Q \quad (16)$$

As we discussed in Section 2, the image systems tabulated in Table 2 and 3 are universally applicable for non-periodic, singly periodic, and doubly periodic geometries, because the Stokes and Laplace monopole kernel sums are designed to be neutral, and the Laplace dipole and quadrupole kernel sums are intrinsically neutral. Also the calculation of gradients and Laplacians ($\nabla_x \boldsymbol{u}^S$, etc.) requires little extra cost in addition to the evaluation of field values ($\boldsymbol{u}^S$, etc.) in both FMM and FFT type methods. In FMM the gradients and Laplacians are straightforward to calculate in the final L2T, S2T and M2T stages because we can directly use the equivalent sources in KIFMM or the multipole basis functions in classic FMM to evaluate the gradients and Laplacians. In FFT type methods the gradients and Laplacians can also be conveniently evaluated using interpolation schemes in the final stage where the kernel sum values are interpolated from the regular FFT mesh to the target points. The detailed cost analysis depends on the specific kernel sum methods used, but in any cases the summation scheme shown in Table 2 and 3 does not change the algorithmic complexity of the underlying kernel sum methods. The final combination stages of Eq. (15) and (16) have negligible cost, similar to the case of the Stokeslet.

We conclude this section with a demonstration of the image system Eq. (16) in the polydisperse case, in the non-periodic geometry above a no-slip wall. The velocity of the target particle with radius a for two cases in Fig. 2: $a/b = 0$ in subplots A & C and $a/b = 0.5$ in subplots B & D, are shown. The no-slip wall is placed at the $x_3 = 0$ plane. The vector field shows the velocity of the target particle, generated by a force $\boldsymbol{F}$ on the source particle b located in $(0, 0, 2b)$. The velocity vectors are colored by their magnitude. $\boldsymbol{F} = (F, 0, 0)$ in A and B, and $\boldsymbol{F} = (0, 0, F)$ in C and D. The dashed circles in B and D have radius $a + b$, showing the region where the center of the target particle cannot enter since we do not allow the source and target spheres to overlap. It is clear that the no-slip condition is satisfied.

5. Discussion & conclusion

In this paper we presented a new image system of a Stokeslet above a no-slip wall. This new image system generates exactly the same flow field in the non-periodic geometry as the image system derived by Blake [8] and by Gimbutas et al. [11]. Moreover, this new image system is straightforward to periodize with the partially periodic kernel summation methods, because the image system has been rearranged into neutral systems. In other words, the periodic (or non-periodic) kernel

sum methods can be called as black-box routines. We demonstrated the accuracy and efficiency of this new image system in Section 3, using the periodic KIFMM by Yan and Shelley [17] as the black-box kernel summation routines. Other summation methods can also be straightforwardly used without modifications [14,29–32].

The decomposition into neutral systems presented in Eq. (2) is not unique. Following the idea of Tornberg and Greengard [21], the summations involving kernels J and G^D can both be represented with several kernel sums involving the Laplace monopole kernel G^S only. This reformulation allows the usage of classic Laplace FMM and Laplace Ewald methods. The Stokeslet image system presented in this work can also be extended to the regularized Stokeslet, by directly integrating Eq. (2) over the regularization 'blob' functions. Then the regularized image system can be periodized, utilizing the doubly periodic schemes by Cortez and Hoffmann [33] for the regularized Stokeslet.

The image systems for other fundamental solutions in Stokes flow have also been studied, including the doublet, stresslet, and rotlet kernels [11]. However they do not need to be rearranged into neutral systems because a doublet, a stresslet, or a rotlet is intrinsically a neutral force couple in Stokes flow.

In this work we also extended our image system of Stokeslet to its Laplacian and the RPY tensor. In both cases the image systems are universally applicable for non-periodic, singly periodic or doubly periodic geometries. The image system for $\nabla_x^2 J$ can be used in the simulations of rigid or flexible fibers above a wall in Stokes flow. The image RPY tensor maintains the Symmetric-Positive-Definiteness of the mobility matrix, and can be widely used in Brownian dynamics simulations where the Brownian fluctuations must be generated from a SPD mobility matrix according to the fluctuation-dissipation theorem.

Acknowledgements

Appendix A. Implementation

The method mentioned in this paper has been implemented in the software `PeriodicFMM`, freely available on GitHub: https://github.com/wenyan4work/PeriodicFMM. The package is native in `C++` with interfaces in `C`, `Fortran`, and `Python`, and is fully parallelized with both `OpenMP` and `MPI`. The package is based on the author's fork of PVFMM [17], also available on GitHub: https://github.com/wenyan4work/pvfmm.

References

[1] P.P. Lele, J.W. Swan, J.F. Brady, N.J. Wagner, E.M. Furst, Colloidal diffusion and hydrodynamic screening near boundaries, Soft Matter 7 (2011) 6844.
[2] V.N. Michailidou, J.W. Swan, J.F. Brady, G. Petekidis, Anisotropic diffusion of concentrated hard-sphere colloids near a hard wall studied by evanescent wave dynamic light scattering, J. Chem. Phys. 139 (2013) 164905.
[3] F. Balboa Usabiaga, B. Delmotte, A. Donev, Brownian dynamics of confined suspensions of active microrollers, J. Chem. Phys. 146 (2017) 134104.
[4] T. Kaya, H. Koser, Direct upstream motility in escherichia coli, Biophys. J. 102 (2012) 1514–1523.
[5] S.E. Spagnolie, E. Lauga, Hydrodynamics of self-propulsion near a boundary: predictions and accuracy of far-field approximations, J. Fluid Mech. 700 (2012) 105–147.
[6] H. Wioland, E. Lushi, R.E. Goldstein, Directed collective motion of bacteria under channel confinement, New J. Phys. 18 (2016) 075002.
[7] B. Ezhilan, D. Saintillan, Transport of a dilute active suspension in pressure-driven channel flow, J. Fluid Mech. 777 (2015) 482–522.
[8] J.R. Blake, A note on the image system for a Stokeslet in a no-slip boundary, Math. Proc. Camb. Philos. Soc. 70 (1971) 303–310.
[9] W.H. Mitchell, S.E. Spagnolie, Sedimentation of spheroidal bodies near walls in viscous fluids: glancing, reversing, tumbling and sliding, J. Fluid Mech. 772 (2015) 600–629.
[10] W.H. Mitchell, S.E. Spagnolie, A generalized traction integral equation for stokes flow, with applications to near-wall particle mobility and viscous erosion, J. Comput. Phys. 333 (2017) 462–482.
[11] Z. Gimbutas, L. Greengard, S. Veerapaneni, Simple and efficient representations for the fundamental solutions of Stokes flow in a half-space, J. Fluid Mech. 776 (2015) R1.
[12] H.-N. Nguyen, K. Leiderman, Computation of the singular and regularized image systems for doubly-periodic Stokes flow in the presence of a wall, J. Comput. Phys. 297 (2015) 442–461.
[13] F. Hoffmann, R. Cortez, Numerical computation of doubly-periodic Stokes flow bounded by a plane with applications to nodal cilia, Commun. Comput. Phys. 22 (2017) 620–642.
[14] D. Lindbo, A.-K. Tornberg, Fast and spectrally accurate summation of 2-periodic Stokes potentials, arXiv:1111.1815 [physics], 2011.
[15] D. Lindbo, A.-K. Tornberg, Fast and spectrally accurate Ewald summation for 2-periodic electrostatic systems, J. Chem. Phys. 136 (2012) 164111.
[16] D.S. Shamshirgar, A.-K. Tornberg, The spectral Ewald method for singly periodic domains, J. Comput. Phys. 347 (2017) 341–366.
[17] W. Yan, M. Shelley, Flexibly imposing periodicity in kernel independent FMM: a multipole-to-local operator approach, J. Comput. Phys. 355 (2018) 214–232.
[18] J. Rotne, S. Prager, Variational treatment of hydrodynamic interaction in polymers, J. Chem. Phys. 50 (1969) 4831–4837.
[19] H. Yamakawa, Transport properties of polymer chains in dilute solution: hydrodynamic interaction, J. Chem. Phys. 53 (1970) 436–443.
[20] H. Hasimoto, On the periodic fundamental solutions of the Stokes equations and their application to viscous flow past a cubic array of spheres, J. Fluid Mech. 5 (1959) 317–328.
[21] A.-K. Tornberg, L. Greengard, A fast multipole method for the three-dimensional Stokes equations, J. Comput. Phys. 227 (2008) 1613–1619.
[22] A.-K. Tornberg, The Ewald sums for singly, doubly and triply periodic electrostatic systems, Adv. Comput. Math. 42 (2015) 227–248.
[23] D. Malhotra, G. Biros, PVFMM: a parallel kernel independent FMM for particle and volume potentials, Commun. Comput. Phys. 18 (2015) 808–830.
[24] L. Ying, G. Biros, D. Zorin, A kernel-independent adaptive fast multipole algorithm in two and three dimensions, J. Comput. Phys. 196 (2004) 591–626.
[25] T. Götz, On collocation schemes for integral equations arising in slender-body approximations of flow past particles with circular cross-section, J. Eng. Math. 42 (2002) 203–221.

[26] E. Nazockdast, A. Rahimian, D. Zorin, M. Shelley, A fast platform for simulating semi-flexible fiber suspensions applied to cell mechanics, J. Comput. Phys. 329 (2017) 173–209.
[27] J. Bleibel, Ewald sum for hydrodynamic interactions with periodicity in two dimensions, J. Phys. A, Math. Theor. 45 (2012) 225002.
[28] J.W. Swan, J.F. Brady, Simulation of hydrodynamically interacting particles near a no-slip boundary, Phys. Fluids 19 (2007) 113306.
[29] D. Lindbo, A.-K. Tornberg, Spectral accuracy in fast Ewald-based methods for particle simulations, J. Comput. Phys. 230 (2011) 8744–8761.
[30] F. Nestler, M. Pippig, D. Potts, Fast Ewald summation based on NFFT with mixed periodicity, J. Comput. Phys. 285 (2015) 280–315.
[31] F. Nestler, An NFFT based approach to the efficient computation of dipole–dipole interactions under various periodic boundary conditions, Appl. Numer. Math. 105 (2016) 25–46.
[32] A.H. Barnett, G. Marple, S. Veerapaneni, L. Zhao, A unified integral equation scheme for doubly-periodic Laplace and Stokes boundary value problems in two dimensions, arXiv:1611.08038 [math], 2016.
[33] R. Cortez, F. Hoffmann, A fast numerical method for computing doubly-periodic regularized Stokes flow in 3D, J. Comput. Phys. 258 (2014) 1–14.